ACS Sustainable Chemistry & Engineering

Research Article

pubs.acs.org/journal/ascecg

Green Synthesis of Carbon- and Silver-Modified Hierarchical ZnO with Excellent Solar Light Driven Photocatalytic Performance

Zhangfeng Shen, Ping Liang, Shaobin Wang, Lihong Liu,* and Shaomin Liu

Department of Chemical Engineering, Curtin University, GPO Box U1987, Perth, Western Australia 6845, Australia

Supporting Information

ABSTRACT: Superstructured ZnO has been the focus of intensive study due to its promising diverse applications. Here, we demonstrate a facile synthesis of hierarchical ZnO particles hybridized with carbon and silver via a simplified bioprocess using yeast mold broth. Better than traditional microbial and biomimetic methods, our microbe-free strategy offers superior ease-of-preparation with minimal negative environmental impact. The relevant reaction parameters including zinc precursor concentration, broth pH value, and broth content were systemically investigated to control the particle morphologies from solid microrod to mesocrystals of porous microcylinder, nanodisk, nanocone, nanoflower, and micro-hamburger. Silver nanoparticles were facilely deposited by photoreduction in the broth. The resultant ZnO@C−Ag composite exhibits a significant improvement in the solar light-irradiated photodegradation of methylene blue solution.

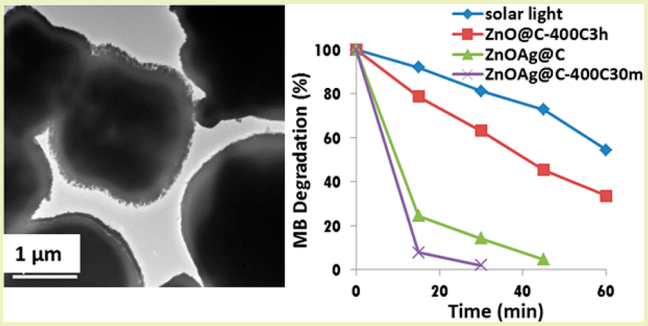

KEYWORDS: *Zinc oxide, Biogenic nanoparticles, Mesocrystal, Green synthesis, Photocatalysis*

INTRODUCTION

Zinc oxide mesocrystals are assemblies of crystallographically oriented ZnO of 0-D quantum dots, 1-D nanowire, or 2-D nanoplates. Superstructured ZnO particles represent a new class of semiconductors that have attracted much attention recently due to their potential applications in fast UV photodetectors and high efficient dye-sensitized solar cell (DSSC) and as the source of terahertz radiation and highly efficient photocatalysis.[1−6] To date, various methods have been developed to synthesize hierarchical ZnO, such as template methods, electrochemical deposition,[7,8] a two-step hydrothermal method,[9] and thermal evaporation techniques.[10] Unfortunately, most of these preparations of ZnO supercrystals are associated with high temperatures, complex procedures, organic solvents, or expensive surfactants.[10−14]

Alternately, advances in biotechnology have led to an environmentally friendly way to prepare ZnO nanocrystals with various green reactants including microorganisms like bacteria and fungi.[15−18] However, developing a biological process to supersede conventional chemical and physical nanosynthesis remains a great challenge due to its low yield, time-consuming microbe isolation, or complicated peptide sequence screening. In addition, certain properties of ZnO are strongly dependent on its extrinsic characteristics, such as morphology, size, and exposed facets, but most of the biogenic ZnO nanoparticles were spherical in nature and enclosed by the less reactive {10−10} facets and therefore have no obvious photocatalytic activity.[19] Although extensive efforts have been made toward the development of a high performance ZnO photocatalyst, there is still plenty of room left unexploited. This is mainly due to the fact that pure ZnO can only be excited by a small UV fraction of solar light. Another challenge is the unfavorable photocorrosion of ZnO under light irradiation, which leads to rapid decline in phtotoactivity and low stability of the photocatalysts. Therefore, forming a heteronanostructure of noble metal or having a residual carbon coating is now an exciting area to improve the photoabsorption efficiency of ZnO in the visible light region and to stabilize the ZnO catalyst. A low loading of Ag on ZnO has increased the photodegradation of methylene blue (MB) and Rhodamine 6G (R_6G) as the Ag clusters respond to the visible light, trap photogenerated electrons, and delay the electron−hole recombination process resulting in higher photocatalytic activity.[20,21] Other research groups have shown that hydrothermal carbon (HTC) originating from biomass and poly- to monosaccharides ideally improved the photostability.[22,23] For instance, Zhang et al. found that the combination of graphite-like carbon and ZnO nanoparticles can suppress the photocorrosion of ZnO.[24] More recently, Qiu's group reported the synthesis of ZnO@C gemel hexagonal microrods by a facile one-step hydrothermal method with furfural as the carbon precursor.[25] Nevertheless, achieving carbon doping and silver nanoparticle formation simultaneously through a green and facile route was scarcely successful.

In our previous studies, yeast mold broth (YMB), a mixture of vitamins, amino acids, proteins, peptone, and dextrose, was utilized to implement fine and accurate control over the

Received: February 26, 2015
Revised: March 20, 2015
Published: March 30, 2015

DOI: 10.1021/acssuschemeng.5b00147
ACS Sustainable Chem. Eng. 2015, 3, 1010−1016

synthesis of Au and Ag nanoparticles.[26,27] In contrast to the conventional biogenic method, this microbe-free approach offers a number of distinct advantages: (1) Nanoparticles can be produced in a larger scale and over shorter periods of time without microorganism involvement. (2) The significantly cheaper costs lies in less expensive raw materials compared to pure peptide, amino acid, or enzyme. Herein, we attempt to explore further this topic by synthesizing 3D hierarchical ZnO structures modified with silver and carbon. Our results in this study demonstrate that monodisperse ZnO twin crystals like microhamburger can be fabricated through a simplified hydrothermal and post-annealing technique. On the basis of electron microscopy, EDX, and XRD analyses, we inferred that YMB may provide proteins and saccharides to compete with OH^- in binding to (0001) facets of ZnO thus facilitating the dipole field-guided orientated attachment of mesocrystals. Meanwhile, dextrose in YMB could be condensed to form an amorphous carbon layer on the surface of ZnO particles as well as to help introduce silver nanoparticles. It was found that this approach leads to a high performance carbon-doped ZnO with a silver heterostructure at the interface for degradation of organic pollutants under solar light.

EXPERIMENTAL SECTION

Sample Preparation. All chemicals were of analytical grade and were used without further purification. Zinc acetate dihydrate ($Zn(CH_3COO)_2{\cdot}2H_2O$), silver nitrate ($AgNO_3$), and sodium hydroxide (NaOH) were purchased from Sigma-Aldrich. Dehydrated yeast mold broth (YMB) was bought from BD Company. All stock solutions were prepared with deionized (DI) water. The aqueous YMB was prepared by suspending 42 or 21 g of the powder in 1 L DI water followed by autoclaving at 121 °C for 15 min.

Carbon-doped ZnO nano- and microparticles (ZnO@C) with different morphologies were synthesized by a simplified hydrothermal method through varying the experimental parameters. In a typical ZnO@C synthesis, pH of the YM broth was first adjusted to a desired value by adding 1 M NaOH solution. After that, zinc acetate aqueous solution, 10 mL, 50 mM, was mixed with 10 mL YM broth under vigorous stirring at room temperature for 5 min. The cloudy reaction mixture in a 100 mL DURAN glass bottle was then autoclaved at 121 °C for 30 to 120 min. Finally, ZnO@C particles were obtained after centrifugation, washed with DI water, and dried in an oven at 50 °C for 5 h. Reference experiments were carried out to evaluate the influences of pH and the reactant contents. For example, the concentration of zinc acetate in the reaction mixture was adjusted from 12.5 to 100 mM to control the size and morphology of the products, in which the other reaction parameters were kept constant. Growth of silver-modified ZnO@C was performed by adding silver nitrate to a ZnO@C solution at a molar ratio of Ag:Zn = 2:100. The final samples were annealed at 400 °C for 30 min in a tube or muffle furnace with or without nitrogen protection.

Characterization. The samples were characterized with an X-ray diffractometer (XRD; Bruker D8 Advance) equipped with Cu Kα radiation (λ = 1.5418 Å). The morphologies of ZnO 3D structures were investigated with a field-emission scanning electron microscope (Zeiss Neon 40EsB FIBSEM). Transmission electron microscope (TEM) images, high-resolution transmission electron microscope (HRTEM) images, and selected area electron diffraction (SAED) patterns were obtained on a JEOL-2010 microscope operated at an accelerating voltage of 200 kV. Samples for TEM characterization were prepared by dropping the colloidal solutions onto a Formvar-coated copper grid and dried in air at room temperature. Fourier transform infrared (FTIR) spectra were measured by using a PerkinElmer Spectrum 100 spectrometer. The Raman spectrum was acquired with a Dilor Labram 1B dispersive Raman spectrometer using a 514.5 nm excitation line. UV–vis absorption spectra of the samples in DI water were recoded using a JASCO V-670 UV–vis/NIR spectrophotometer. Thermogravimetric analysis (TGA; Mettler-Toledo) was performed using a simultaneous differential thermal analysis (DTA). A heating rate of 5 °C/m from room temperature to 900 °C was used under an air atmosphere. Elemental analysis was performed by using a PerkinElmer 2400 Series II CHNS/O elemental analyzer.

Photocatalytic Test. Methylene blue (MB) was chosen as a probe molecule to evaluate the performance of ZnO@C and ZnO@C–Ag. The photocatalytic degradation of MB was carried out in a glass beaker under AM 1.5 100 mW/cm^2 simulated sunlight (550W, xenon lamp, ABET Technologies, Model 11016A Sun 3000). In a typical experiment, 15.0 mg of photocatalyst was dispersed in 15 mL, 1.0 × 10^{-5} M MB solution. The mixed suspensions were magnetically stirred for 30 min in the dark to reach an adsorption–desorption equilibrium of MB onto the ZnO catalyst. At certain time intervals of irradiation, 0.8 mL of the suspension was withdrawn and centrifuged to remove ZnO particles. The reaction process was followed by measuring the absorption of MB in the filtrate at 664 nm. The reusability of ZnO@C–Ag was tested by three successive cycles for the degradation of MB. After each cycle, the particles were centrifuged and redispersed into fresh MB solution without further treatment.

RESULTS AND DISCUSSION

Morphology and Structure Characterization of ZnO Particles. To assess the effect of yeast mold broth (YMB), control samples (without addition of YMB) were first prepared by mixing 50 mM of zinc acetate (10 mL), DI water (10 mL) and a certain amount of 1 M sodium hydroxide solution according to the procedure described in the Eperimental Section. The samples with the total volume of NaOH at 500, 1000, and 1500 μL were denoted as 25ZnDI500, 25ZnDI1000, and 25ZnDI1500, respectively. Figure 1A shows that the as-prepared 25ZnDI500 consists of hexagonally prismatic microrods. The rods have lengths of 0.5–2 μm and diameters of about 0.4 μm. Some microrods are broken and truncated. In this reaction system, pH is the key factor influencing the morphology of the ZnO particles. Figure 1B reveals the image of 25ZnDI1000 in nanocones. When NaOH volume was increased to 1500 μL, irregular nanograins of ZnO were obtained (Figure 1C). The XRD patterns of corresponding samples are shown in Figure 1D–F. In all cases, a highly crystalline wurtzite phase was identified (JSCPS card No. 36-1451). The relatively broader widths of the diffraction peaks in

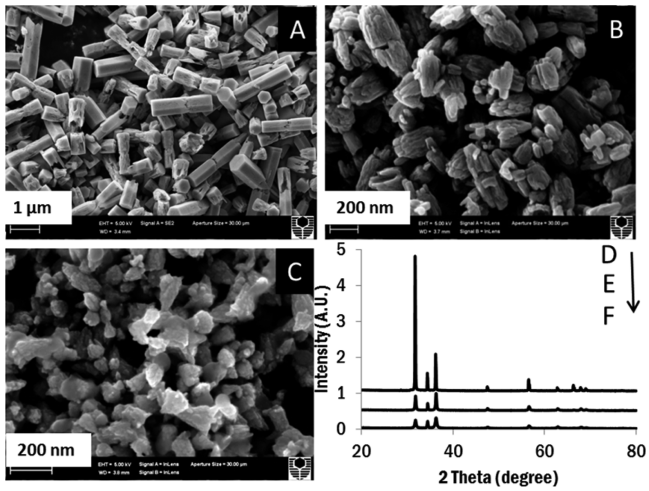

Figure 1. SEM images and XRD patterns of ZnO products synthesized in deionized water with increasing ratios of $[OH^-]/[Zn^{2+}]$ from 1:1 (A,D, 25ZnDI500) to 2:1 (B,E, 25ZnDI1000) to 3:1 (C,F, 25ZnDI1500).

DOI: 10.1021/acssuschemeng.5b00147
ACS Sustainable Chem. Eng. 2015, 3, 1010–1016

Figures 1E and F indicate the formation of smaller ZnO crystallites. These results are consistent with ZnO single crystal growth behavior in an aqueous solution as reported by Li et al.[28] The authors defined the generally accepted reaction routes in an alkali medium as follows

$$Zn^{2+} + 4OH^- \rightarrow Zn(OH)_4^{2-} \quad (1)$$

$$Zn(OH)_4^{2-} \rightarrow ZnO + H_2O + 2OH^- \quad (2)$$

In their hydrothermal experiments, smaller nanograins were formed due to the larger shielding effect of OH^- ions at the interface of the (0001) planes; the growth rate along *c*-axis was significantly decreased relative to other directions.

It is well known that the wurtzite ZnO structure with alternating polar surfaces of Zn^{2+}-terminated (0001) and O^{2-}-terminated ($000\bar{1}$) along the *c*-axis offers an intrinsic dipole moment and easy growth of hierarchical superstructures, such as spheroidal ZnO aggregates, nanocones, twin-brush, and so on.[29−32] Synthetic surfactants like cetyltrimethylammonium bromide (CTAB), Triton X-100, sodium dodecyl sulfate (SDS), and sodium bis(2-ethylhexyl) sulfosuccinate (NaAOT) were most frequently employed to mediate 3D ZnO assembly.[33−35] Recently, the biomimetic approach toward the synthesis of zinc oxide has attracted a growing interest due to its advantages of mild conditions and easiness of handling. Pure amino acids,[36−38] artificial peptides with an affinity for ZnO,[18] gelatin,[39] and proteins secreted by zinc metal tolerant soil fungus[16] have been reported toward the development of an environmentally benign protocol for fabrication of ZnO nanoparticles. A number of ZnO assemblies have been mediated with natural polysaccharides, such as pectin,[40] hyaluronic acid, and chondroitin-6-sulfate.[41] Gum arabic, a complex mixture of glycoproteins and highly branched polysaccharides, has been successfully employed to guide the evolution of twin-brush ZnO mesocrystals.[32] On the basis of our previous works, we note that yeast mold broth powder, not only rich in various amino acids but also containing 0.3 wt % *Saccharomyces cerevisiae* yeast extract and thus abundant in yeast polysaccharide mannan, should have the potential to promote secondary ZnO aggregation.

As part of our ongoing efforts to synthesize environmentally friendly nanoparticles, ZnO particles were also prepared in the presence of 1× YMB (21 g YMB powder in 1 L DI water). FESEM images of ZnO samples with varying 1 M NaOH volume are shown in Figure 2. The addition of 500 μL of NaOH solution resulted in pure and uniform nanodisks (25ZnYM500) with diameters around 1 μm. Li et al. fabricated similar hexagonal-based thin disks by employing an oil-in-water microemulsion method.[35] The formation of the hexagonal disks is suggested to be due to the self-assembly of the NaAOT template. Recently, a template-free method using butanol as the reaction solvent has been demonstrated to obtain ZnO mesocrystals after 12 h reaction at 120 °C.[42] Butanol or H_2O adsorbed on the (0001) planes has been proposed to induce the energetically unfavorable growth of ZnO microspheres. In our study, we hypothesize that amino acids or other functional groups from the YMB may compete with OH^- in binding to the ZnO (0001) surface and suppress the growth along the *c*-axis. As the volume of NaOH solution increased to 1000 and 1500 μL, although the 25ZnYM1000 and 25ZnYM1500 crystals still maintain comparable size as 25ZnDI1000 and 25ZnDI1500, the surfaces of the ZnO particles become rougher and nanostrawberries and nanoflowers with grainy surfaces

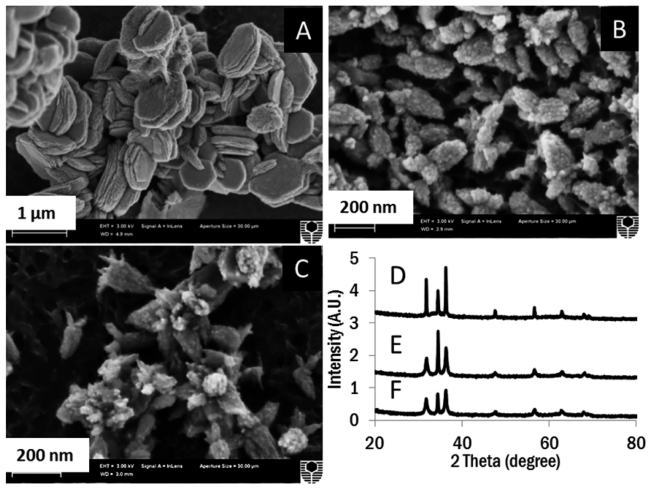

Figure 2. SEM images and XRD patterns of ZnO particles prepared in the presence of 1× yeast mold broth (21 g yeast mold broth powder in 1 L DI water) with increasing ratios of $[OH^-]/[Zn^{2+}]$ from 1:1 (A,D, 25ZnYM500) to 2:1 (B,E, 25ZnYM1000) to 3:1 (C,F, 25ZnYM1500).

were formed, respectively. These results illustrate that YMB components clearly assist in the oriented attachment of primary ZnO nanoparticles, thus leading to the formation of the superstructures.

To test the influence of zinc precursor concentration, $[OH^-]$ was fixed at 17 mM, while $[Zn^{2+}]$ was increased from 12.5 to 100 mM in 1× YMB. Figure 3 presents the variation of the particle thickness, morphology, and size with increasing $Zn(OAc)_2$ concentration. Clearly, we can see that thin nanoplatelets, twin-nanodisks, thick microdonuts, and micro-apples were predominately formed at a $[Zn^{2+}]$ of 12.5, 25, 50, and 100 mM, respectively. A close examination reveals the particle surface is composed of loosely packed nanoplatelets with sizes of 30−50 nm. It is worth noting the coexistence of graphene-like sheets. As shown in Figure 3D, the surface of the ZnO particle is wrapped by sheets.

TEM investigations were performed on samples obtained from 1× YMB with 50 mM of $[Zn^{2+}]$ and 17 mM of $[OH^-]$ after 60 min reaction. The HRTEM image in Figure 4D shows the lattice fringe with a 0.26 nm *d*-spacing for the (002) reflection.[43] A selected area electron diffraction (SAED) pattern indicates that the microdonuts are single crystalline (Figure 4E). Graphene-like sheets (Figure 4B) are amorphous as indicated by SAED pattern in Figure 4C.

So far, we have confirmed the structure-directing function of YMB powder. However, the synthesis of a relatively uniform and high quality ZnO mesocrystal has not been successful. It is well reported in the literature that crystal development is largely dependent on the dosage of morphology mediation agents. Therefore, we systematically investigated the influence of the concentration of YMB powder. In the presence of 2× YMB (42 g YMB powder in 1 L DI water, 4.2%), only amorphous black powder was obtained after a 2 h reaction at 121 °C. From Figure S1A of the Supporting Information, we can see that the sample consists of microspheres with the diameter ranging from 0.3 to 1 μm in coexistence with primary nanoparticles with sizes around 10 nm. Decreasing the content of YMB from 4.2 to 2.1%, crystalline ZnO particles of varying sizes and shapes were revealed (Figure S1B, Supporting Information). Interestingly, highly porous and crystalline microcylinders were formed by using 1.05% YMB solution. A high magnification SEM inset

DOI: 10.1021/acssuschemeng.5b00147
ACS Sustainable Chem. Eng. 2015, 3, 1010−1016

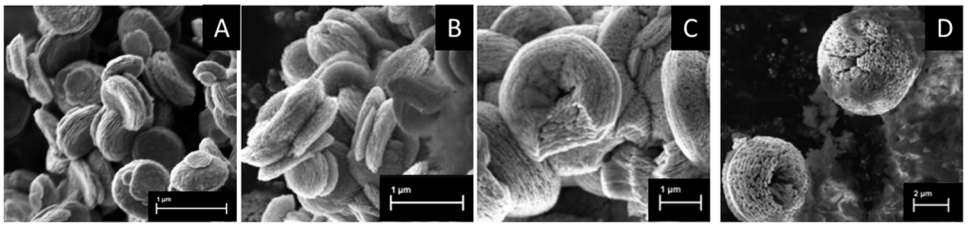

Figure 3. SEM images of ZnO products synthesized with increasing $[Zn^{2+}]$ from 12.5 mM (A), 25 mM (B), 50 mM (C), to 100 mM (D). The concentration of NaOH was maintained the same at 17 mM in the reaction solution. All samples were prepared with the presence of 1× yeast mold broth.

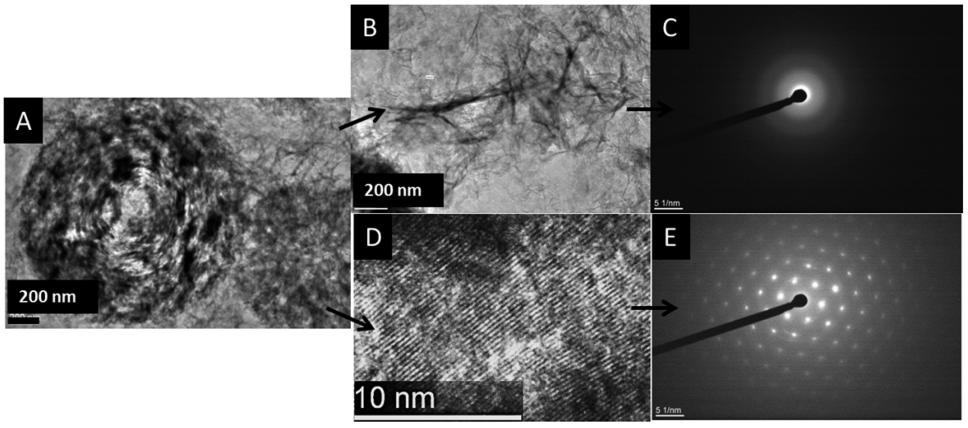

Figure 4. TEM images of ZnO particles enwrapped with amorphous hydrothermal carbon. The final concentration of OH^- and Zn^{2+} was 17 and 50 mM, respectively, in 1× yeast mold broth.

reveals that the cylinder consists of packed nanocrystallites. Up to now, most advantageous and porous ZnO superstructures were prepared by calcining a precursor at high temperature.[44,45] To the best of our knowledge, this is the first report on porous ZnO fabrication at such low temperature (121 °C) in just 1 h and without addition of any template, which is much more facile than previous reports.[46,47]

YMB powder is sugar rich, which is composed of 47.6% dextrose, 14.3% yeast extract, 23.8% peptone, and 14.3% malt extract. We hypothesize that, under hydrothermal conditions, the dextrose and mannan may follow a chemical reaction path, like the dehydration of sugar, where there is formation of 5-hydroxymethyl-furfural-aldehyde (HMF) and subsequent transformation to hydrothermal carbon.[48] This view is supported by SEM characterization. Morphology of black powder in Figure S1A of the Supporting Information is quite similar to the SEM images of hydrothermal carbons prepared using glucose and HMF as precursors. Moreover, a high concentration of organic acids (acetic, lactic, propenoic, levulinic, and formic acids) derived from the decomposition of sugars[49] in 2× YMB may competitively react with NaOH thus suppressing the formation of $Zn(OH)_4^{2-}$ and ZnO particles. Although 0.5× YMB and addition of 340 μL of 1 M NaOH ($[OH^-]/[Zn^{2+}]$ = 17:25) produces ZnO microparticles with intensified and sharp diffraction peaks, they are still partially covered by a certain amount of laminar precipitations, which indicates that NaOH is insufficient and the hydrothermal carbon has exceeded the amount needed to thinly cover the ZnO particles. By increasing the NaOH addition to 500 μL ($[OH^-]/[Zn^{2+}]$ = 1:1), we finally obtained thin hydrothermal carbon (HTC)-coated ZnO samples named ZnO@C.

FTIR spectroscopy was used to determine the functional groups contributing to ZnO assemblies (Figure S2, Supporting Information). YMB shows expected absorption bands including (1) the highest intensity of the ν (OH) band at 3372 cm^{-1}, (2) $\nu_{asym}(CH_2)$ lipids at 2925 cm^{-1},[50] (3) the presence of amide I band at 1636 cm^{-1} arising from C═O stretching and contribution of N−H bending,[51] (4) 1552 cm^{-1}, amide II band of δ_{N-H} or ν_{C-N} vibrations in different protein conformations, (5) 1405 cm^{-1}, s, δ_{CH3} stretching mainly in proteins, (6) 1390 cm^{-1}, C═O of COO^- symmetric stretching in proteins, (7) 1350 cm^{-1},CH_2 wagging vibrations in lipids, (8) 1042 cm^{-1}, $\beta(1 \rightarrow 3)$ glucans, and (9) 828 cm^{-1}, mannans.[50] These bands could be found in the FTIR spectra of ZnO@C samples, indicating the involvement of proteins and mannans in the synthesis process.

The optical properties of the as-synthesized ZnO nanostructures were further characterized by UV−vis measurements at room temperature. Figure S3 of the Supporting Information shows the extinction spectra of ZnO particles. For the control samples without the addition of YMB powder, a weak absorption peak appears at 367 nm. With the presence of YMB powder, the blue-shifted absorption becomes intense, and the absorption peak is wider than its counterpart.

Silver-Modified ZnO@C Samples. The Ag-modified ZnO@C samples denoted as ZnO@C−Ag were synthesized by mixing $AgNO_3$ and ZnO@C solution under a sun simulator with irradiation for 5 min. After centrifugation, the products were annealed at 400 °C in air for 30 min. There is virtually no change in the morphology, particle size, and crystalline phase after Ag modification, as confirmed by the TEM/SEM micrographs and XRD patterns (Figure 5). All major peaks in the diffraction patterns match with those of a typical wurtzite ZnO. The peaks at 2θ values of 38.1°, 44.4°, and 64.4° were attributed to crystal planes of metallic Ag (JCPDS file: 65-2871). The silver modifying does not cause diffraction peaks

DOI: 10.1021/acssuschemeng.5b00147
ACS Sustainable Chem. Eng. 2015, 3, 1010−1016

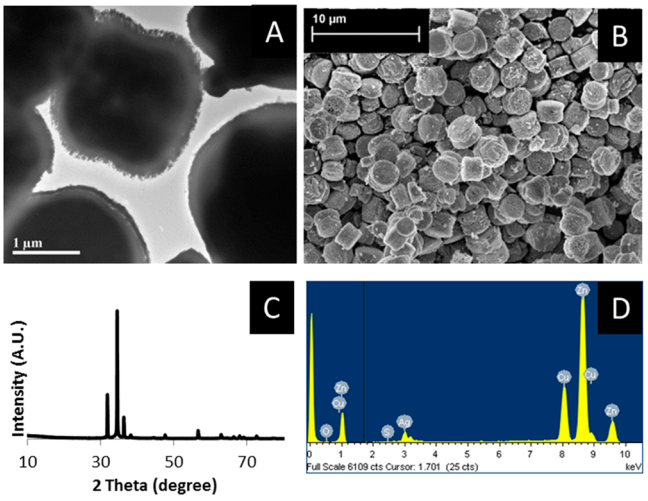

Figure 5. (A) TEM images showing the microhamburger morphology of the ZnO@C−Ag particles, (B) SEM images, (C) XRD pattern of ZnO and Ag NPs, and (D) EDX analysis of ZnO@C−Ag after annealing at 400 °C for 30 min.

shift of ZnO, implying that Ag simply clusters on the surface of ZnO rather than substituting for the Zn^{2+} and going into the lattice of ZnO, due to the big difference between the radius of Ag^{+} and Zn^{2+}.[52] The presence of Ag, carbon, and ZnO was further revealed by EDS, HRTEM, and Raman analysis (Figure 5D and Figures S4 and S5, Supporting Information).

Elemental analysis was carried out for the ZnO@C and ZnO@C−Ag samples (Table S1, Supporting Information). C and N contents in YMB powder are 40.9% and 6.3%, respectively. The samples prepared in 4.2, 2.1, and 1.05% YMB solution are named YMZnO@C, 0.5YMZnO@C, and 0.25YMZnO@C, and their C content decreased from 9.1% to 3.8% and 2.3%, indicating that the C is from hydrothermal decomposition of YMB powder mainly. After annealing 0.5YMZn@C in air and N_2, the content of C dropped to 0.8% and 1.7%, respectively. Ag incorporating has no obvious influence on the carbon content of the samples as confirmed by the C content of 0.5YMZn@C and 0.5YMZn@C−Ag at 3.8% and 4.0%, respectively. The weight percentage of the carbon in thermally annealed ZnO@C−Ag_400C30m sample (400 °C for 30 min in air) is 0.9%.

TGA analysis further reveals the trend of decreased hydrothermal carbon (HTC) in the ZnO@C−Ag composites as shown in Figure 6. It was clear that the weight loss of HTC started from 220 °C and continuously decreased up to 500 °C due to the combustion of carbon on the sample surface.[25] It is worth noticing that the weight loss percentage of all samples was higher than the C content as indicated by elemental analysis. The extra weight loss may be due to the decomposition of Ag_2O in ZnO system.[52] Ag_2O has been reported to be stable at 300 °C but decomposes to metallic silver at 400 °C. The result is consistent with better photocatalytic performance of annealed samples as discussed in the following section.

Photocatalytic activity and reusability. The photodegradation of MB catalyzed by different ZnO samples under solar light is shown in Figure 7. To screen the catalysts efficiently, MB solution at low concentration (1×10^{-5} M) was employed. Although the blank experiment shows a self-photodegradation of MB under solar light, the catalyst samples exhibit enhanced degradation efficiency. Nevertheless, the

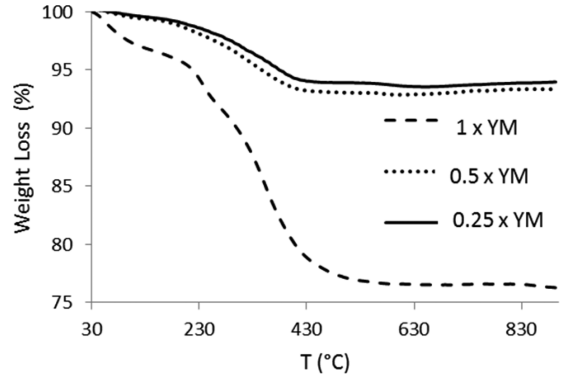

Figure 6. TGA curves of thermal decomposition of ZnO@C−Ag prepared with different concentration of yeast mold broth powder.

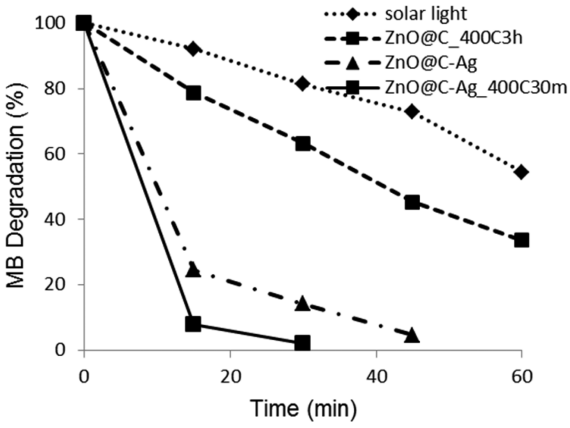

Figure 7. Photocatalytic degradation of methylene blue under solar light irradiation over different ZnO samples.

ZnO@C samples without post-annealing treatment exhibited little positive effect due to a high content of carbon that shields the light on the surface of ZnO photocatalyst. Similarly, ZnO@C−Ag annealed in N_2 exhibited lower activity compared to the countparts annealed in air (data not show).[53] For a clear view, we presented MB degradation profiles on several typical samples only. When exposed to solar light, about 66% of MB can be degraded by ZnO@C_400C3h after 60 min. ZnO@C−Ag degraded nearly 100% MB in 60 min. The annealed ZnO@C−Ag_400C30m ternary composite shows the best performance, evidenced by the fact that nearly 100% MB has been degraded in 15 min. It is known that efficient light absorption and charge transportation and separation are crucial factors in enhancing the photocatalytic performance. Ag nanoparticles have been reported as "electron reservoirs" and effectively prolong the lifetime of the photogenerated electron−hole pairs thus leading to a remarkably improved photoactivity.

To evaluate the photostability of the catalysts, three successive cyclic MB degradation tests under solar light were carried out, and it is found that ZnO@C−Ag_400C30m remains 96% photocatalytically efficienct after three recycles, indicating no serious corrosion of ZnO due to the hybridized HTC coating layer.

In summary, we present a green method for rapid growth of high-quality ZnO nanomicrostructures enwrapped with a thin carbon layer. By optimizing the reaction parameters, ZnO@C of various sizes and shapes have been produced through a hydrothermal process with yeast mold broth powder as both the carbon precursor and directing agent of ZnO nucleation.

DOI: 10.1021/acssuschemeng.5b00147
ACS Sustainable Chem. Eng. 2015, 3, 1010−1016

Subsequently, the ZnO@C−Ag composites have been facilely prepared and have demonstrated excellent photocatalytic activities.

■ ASSOCIATED CONTENT

Supporting Information

Effect of yeast mold broth concentration on the formation of ZnO mesocrystals, typical FTIR spectra of yeast mold broth powder and ZnO@C samples, UV−visible absorption spectra of ZnO particles prepared in DI water and in yeast mold broth, and HRTEM and Raman spectrum of the ZnO@C−Ag sample. Table S1 lists the synthesis conditions and chemical compositions of ZnO products. This material is available free of charge via the Internet at http://pubs.acs.org.

■ AUTHOR INFORMATION

Corresponding Author

*E-mail: Lihong·Liu@curtin.edu.au. Tel: 61-8-92669201. Fax: 61-8-92662681.

Author Contributions

The manuscript was written through contributions of all authors. All authors have given approval to the final version of the manuscript.

Notes

The authors declare no competing financial interest.

■ ACKNOWLEDGMENTS

This work was partially supported by the Australian Research Council (DP110104599 and DP150103026). Electron microscopy characterizations were performed in the Electron Microscope Facility of Curtin University. The authors acknowledge the provision of research facilities and the scientific and technical assistance of the staff of CHIRI Biosciences Research Precinct core facility, Curtin University. The authors appreciate the great support from Dr. X. Wang, G. Zhou, E. Miller, X. Hua, A. Werner, and Dr. R. Steuart.

■ REFERENCES

(1) Li, Y.; Duan, G.; Liu, G.; Cai, W. Physical processes-aided periodic micro/nanostructured arrays by colloidal template technique: fabrication and applications. *Chem. Soc. Rev.* **2013**, *42*, 3614−3627.

(2) Li, Y.; Koshizaki, N.; Wang, H.; Shimizu, Y. Untraditional approach to complex hierarchical periodic arrays with trinary stepwise architectures of micro-, submicro-, and nanosized structures based on binary colloidal crystals and their fine structure enhanced properties. *ACS Nano* **2011**, *5*, 9403−9412.

(3) Gedamu, D.; Paulowicz, I.; Kaps, S.; Lupan, O.; Wille, S.; Haidarschin, G.; Mishra, Y. K.; Adelung, R. Rapid fabrication technique for interpenetrated ZnO nanotetrapod networks for fast UV sensors. *Adv. Mater.* **2014**, *26*, 1541−1550.

(4) Shi, Y.; Wang, K.; Du, Y.; Zhang, H.; Gu, J.; Zhu, C.; Wang, L.; Guo, W.; Hagfeldt, A.; Wang, N.; Ma, T. Solid-state synthesis of ZnO nanostructures for quasi-solid dye-sensitized solar cells with high efficiencies up to 6.46%. *Adv. Mater.* **2013**, *25*, 4413−4419.

(5) Wu, X. L.; Xiong, S. J.; Liu, Z.; Chen, J.; Shen, J. C.; Li, T. H.; Wu, P. H.; Chu, P. K. Green light stimulates terahertz emission from mesocrystal microspheres. *Nat. Nanotechnol.* **2011**, *6*, 103−106.

(6) Wang, M.; Zhang, Y.; Zhou, Y.; Yang, F.; Kim, E.; Hahn, S.; Seong, S. Rapid room-temperature synthesis of nanosheet-assembled ZnO mesocrystals with excellent photocatalytic activity. *CrystEngComm.* **2013**, *15*, 754−763.

(7) Dong, Z.; Lai, X.; Halpert, J. E.; Yang, N.; Yi, L.; Zhai, J.; Wang, D.; Tang, Z.; Jiang, L. Accurate control of multishelled ZnO hollow microspheres for dye-sensitized solar cells with high efficiency. *Adv. Mater.* **2012**, *24*, 1046−1049.

(8) Elias, J.; Lévy-Clément, C.; Bechelany, M.; Michler, J.; Wang, G.; Wang, Z.; Philippe, L. Hollow urchin-like ZnO thin films by electrochemical deposition. *Adv. Mater.* **2010**, *22*, 1607−1612.

(9) Guo, H.; He, X.; Hu, C.; Hu, Y.; Xi, Y.; Chen, J.; Li, T. Effect of particle size in aggregates of ZnO-aggregate-based dye-sensitized solar cells. *Electrochim. Acta* **2014**, *120*, 23−29.

(10) Kong, X. Y.; Ding, Y.; Yang, R.; Wang, Z. L. Single-crystal nanorings formed by epitaxial self-coiling of polar nanobelts. *Science* **2004**, *303*, 1348−1351.

(11) Tang, G.; Tian, S.; Zhou, Z.; Wen, Y.; Pang, A.; Zhang, Y.; Zeng, D.; Li, H.; Shan, B.; Xie, C. ZnO micro/nanocrystals with tunable exposed (0001) facets for enhanced catalytic activity on the thermal decomposition of ammonium perchlorate. *J. Phys. Chem. C* **2014**, *118*, 11833−11841.

(12) Mclaren, A.; Valdes-Solis, T.; Li, G.; Tsang, S. C. Shape and size effects of ZnO nanocrystals on photocatalytic activity. *J. Am. Chem. Soc.* **2009**, *131*, 12540−12541.

(13) Li, P.; Wang, D.; Wei, Z.; Peng, Q.; Li, Y. Systematic synthesis of ZnO nanostructures. *Chem.—Eur. J.* **2013**, *19*, 3735−3740.

(14) Li, F.; Ding, Y.; Gao, P.; Xin, X.; Wang, Z. Single-crystal hexagonal disks and rings of ZnO: low-temperature, large-scale synthesis and growth mechanism. *Angew. Chem., Int. Ed.* **2004**, *116*, 5350−5354.

(15) Wang, A. J.; Liao, Q.; Feng, J.; Zhang, P.; Lia, A.; Wang, J. Apple pectin-mediated green synthesis of hollow double-caged peanut-like ZnO hierarchical superstructures and photocatalytic applications. *CrystEngComm* **2012**, *14*, 256−263.

(16) Jain, N.; Bhargava, A.; Tarafdar, J. C.; Singh, S. K.; Panwar, J. A biomimetic approach towards synthesis of zinc oxide nanoparticles. *Appl. Microbiol. Biotechnol.* **2013**, *97*, 859−869.

(17) Hussein, M. Z.; Azmin, W. H. W. N.; Mustafa, M.; Yahaya, A. H. Bacillus cereus as a biotemplating agent for the synthesis of zinc oxide with raspberry- and plate-like structures. *J. Inorg. Biochem.* **2009**, *103*, 1145−1150.

(18) Umetsu, M.; Mizuta, M.; Tsumoto, K.; Ohara, S.; Takami, S.; Watanabe, H.; Kumagai, I.; Adschiri, T. Bioassisted room-temperature immobilization and mineralization of zinc oxide—The structural ordering of ZnO nanoparticles into a flower-type morphology. *Adv. Mater.* **2005**, *17*, 2571−2575.

(19) Jayaseelan, C.; Abdul Rahuman, A.; Kirthi, A. V.; Marimuthu, S.; Santhoshkumar, T.; Bagavan, A.; Gaurav, K.; Karthik, L.; Rao, K.V. B. Novel microbial route to synthesize ZnO nanoparticles using *Aeromonas hydrophila* and their activity against pathogenic bacteria and fungi. *Spectrochim. Acta. A* **2012**, *90*, 78−84.

(20) Height, M.; Pratsinis, S.; Mekasuwandumrong, O.; Praserthdam, P. Ag-ZnO catalysts for UV-photodegradation of methylene blue. *Appl. Catal., B* **2006**, *63*, 305−312.

(21) Georgekutty, R.; Seery, M.; Pillai, S. A highly efficient Ag-ZnO photocatalyst: Synthesis, properties, and Mechanism. *J. Phys. Chem. C* **2008**, *112*, 13563−13570.

(22) Titirici, M.; Antonietti, M.; Baccile, N. Hydrothermal carbon from biomass: A comparison of the local structure from poly- to monosaccharides and pentoses/hexoses. *Green Chem.* **2008**, *10*, 1204−1212.

(23) Sun, X.; Li, Y. Colloidal carbon spheres and their core/shell structures with noble-metal nanoparticles. *Angew. Chem., Int. Ed.* **2004**, *43*, 597−601.

(24) Zhang, L.; Cheng, H.; Zong, R.; Zhu, Y. Photocorrosion suppression of ZnO nanoparticles via hybridization with graphite-like carbon and enhanced photocatalytic activity. *J. Phys. Chem. C* **2009**, *113*, 2368−2374.

(25) Zhang, P.; Li, B.; Zhao, Z.; Yu, C.; Hu, C.; Wu, S.; Qiu, J. Furfural-induced hydrothermal synthesis of ZnO@C gemel hexagonal microrods with enhanced photocatalytic activity and stability. *ACS Appl. Mater. Interfaces* **2014**, *6*, 8560−8566.

DOI: 10.1021/acssuschemeng.5b00147
ACS Sustainable Chem. Eng. 2015, 3, 1010−1016

(26) Liu, L.; Shao, Z.; Ang, M.; Tade, M.; Liu, S. Are microorganisms indispensable in green microbial nanomaterial synthesis? *RSC Adv.* **2014**, *4*, 14564−14568.
(27) Liu, L.; Liu, T.; Tade, M.; Wang, S.; Li, X.; Liu, S. Less is more, greener microbial synthesis of silver nanoparticles. *Enzyme Microb. Technol.* **2014**, *67*, 53−58.
(28) Li, W.; Shi, E.; Zhong, W.; Yin, Z. Growth mechanism and growth habit of oxide crystals. *J. Cryst. Growth* **1999**, *203*, 186−196.
(29) Distaso, M.; Klupp Taylor, R. N.; Taccardi, N.; Wasserscheid, P.; Peukert, W. Influence of the counterion on the synthesis of ZnO mesocrystals under solvothermal conditions. *Chem.—Eur. J.* **2011**, *17*, 2923−2930.
(30) Wu, D.; Gao, Z.; Xu, F.; Chang, J.; Tao, W.; He, J.; Gao, S.; Jiang, K. Hierarchical ZnO aggregates assembled by orderly aligned nanorods for dye-sensitized solar cells. *CrystEngComm* **2013**, *15*, 1210−1217.
(31) Klaumünzer, M.; Distaso, M.; Hübner, H.; Mačković, M.; Spiecker, E.; Kryschi, C.; Peukert, W. ZnO superstructures via oriented aggregation initiated in a block copolymer melt. *CrystEngComm* **2014**, *16*, 1502−1513.
(32) Liu, M.; Tseng, Y.; Greer, H. F.; Zhou, W.; Mou, C. Dipole field guided orientated attachment of nanocrystals to twin-brush ZnO mesocrystals. *Chem.—Eur. J.* **2012**, *18*, 16104−16113.
(33) Tang, H.; Chang, J. C.; Shan, Y.; Lee, S. Surfactant-assisted alignment of ZnO nanocrystals to super structures. *J. Phys. Chem. B* **2008**, *112*, 4016−4021.
(34) Jung, M.; Chu, M. Synthesis of hexagonal ZnO nanodrums, nanosheets and nanowires by the ionic effect during the growth of hexagonal ZnO crystals. *J. Mater. Chem. C* **2014**, *2*, 6675−6682.
(35) Li, F.; Ding, Y.; Gao, P.; Xin, X.; Wang, Z. Single-crystal hexagonal disks and rings of ZnO: low-temperature, large-scale synthesis and growth mechanism. *Angew. Chem.* **2004**, *116*, 5350−5354.
(36) Subramanian, N.; Ghaferi, A. A. An amino acid-based swift synthesis of zinc oxide nanostructures. *RSC Adv.* **2014**, *4*, 4371−4378.
(37) Brif, A.; Ankonina, G.; Drathen, C.; Pokroy, B. Bio-inspired band gap engineering of zinc oxide by intracrystalline incorporation of amino acids. *Adv. Mater.* **2014**, *26*, 477−481.
(38) Ramani, M.; Ponnusamy, S.; Muthamizhchelvan, C.; Marsili, E. Amino acid-mediated synthesis of zinc oxide nanostructures and evaluation of their facet-dependent antimicrobial activity. *Colloids Surf., B* **2014**, *117*, 233−239.
(39) Tseng, Y.; Liu, M.; Kuo, Y.; Chen, P.; Chen, C.; Chen, Y.; Mou, C. Biomimetic ZnO plate twin-crystals periodical arrays. *Chem. Commun.* **2012**, *48*, 3215−3217.
(40) Wang, A.; Liao, Q.; Feng, J.; Zhang, P.; Lia, A.; Wang, J. Apple pectin-mediated green synthesis of hollow double-caged peanut-like ZnO hierarchical superstructures and photocatalytic applications. *CrystEngComm* **2012**, *14*, 256.
(41) Waltz, F.; Wißmann, G.; Lippke, J.; Schneider, A. M.; Schwarz, H.; Feldhoff, A.; Eiden, S.; Behrens, P. Evolution of the morphologies of zinc oxide mesocrystals under the influence of natural polysaccharides. *Cryst. Growth Des.* **2012**, *12*, 3066−3075.
(42) Wang, S.; Xu, A. Template-free facile solution synthesis and optical properties of ZnO mesocrystals. *CrystEngComm* **2013**, *15*, 376−381.
(43) Ge, M. Y.; Wu, H. P.; Niu, L.; Liu, J. F.; Chen, S. Y.; Shen, P. Y.; Zeng, Y. W.; Wang, Y. W.; Zhang, G. Q.; Jiang, J. Z. Nanostructured ZnO: From monodisperse nanoparitcles to nanorods. *J. Cryst. Growth* **2007**, *305*, 162−166.
(44) Song, R. Q.; Xu, A. W.; Deng, B.; Li, Q.; Chen, G. Y. From layered basic zinc acetate nanobelts to hierarchical zinc oxide nanostructures and porous zinc oxide nanobelts. *Adv. Funct. Mater.* **2007**, *17*, 296−306.
(45) Yang, Y.; Yang, Y.; Wu, H.; Guo, S. Control of the formation of rod-like ZnO mesocrystals and their photocatalytic properties. *CrystEngComm* **2013**, *15*, 2608−2615.
(46) Dong, L.; Tang, S.; Zhu, J.; Xia, G. From one nanobelt precursor to different ZnO nano/micro structures: porous nanobelts self-standing film and microtubes. *CrystEngComm* **2013**, *15*, 9916−9922.
(47) Yin, J.; Gao, F.; Wei, C.; Lu, Q. Water amount dependence on morphologies and properties of ZnO nanostructures in double-solvent system. *Sci. Rep.* **2014**, *4*, 3736 DOI: 10.1038/srep03736.
(48) Titirici, M.; Antoniettia, M.; Baccile. Hydrothermal carbon from biomass: a comparison of the local structure from poly- to monosaccharides and pentoses/hexoses. *Green Chem.* **2008**, *10*, 1204−1212.
(49) Sevilla, M.; Fuertes, A. B. The production of carbon materials by hydrothermal carbonization of cellulose. *Carbon* **2009**, *47*, 2281−2289.
(50) Cavagna, M.; Dell'Anna, R.; Monti, F.; Rossi, F.; Torriani, S. Use of ATR-FTIR microspectroscopy to monitor autolysis of *Saccharomyces cerevisiae* cells in a base wine. *J. Agric. Food Chem.* **2010**, *58*, 39−45.
(51) Galichet, A.; Sockalingum, G. D.; Belarbi, A.; Manfait, M. FTIR spectroscopic analysis of Saccharomyces cerevisiae cell walls: Study of an anomalous strain exhibiting a pink-colored cell phenotype. *FEMS Microbiol. Lett.* **2001**, *197*, 179−186.
(52) Georgekutty, R.; Seery, M.; Pillai, S. A highly efficient Ag−ZnO photocatalyst: Synthesis, properties, and mechanism. *J. Phys. Chem. C* **2008**, *112*, 13563−13570.
(53) Liu, J.; Zhang, Q.; Yang, J.; Ma, H.; Tade, M. O.; Wang, S.; Liu, J. Facile synthesis of carbon-doped mesoporous anatase TiO_2 for the enhanced visible-light driven photocatalysis. *Chem. Commun.* **2014**, *50*, 13971−13974.

DOI: 10.1021/acssuschemeng.5b00147
ACS Sustainable Chem. Eng. 2015, 3, 1010−1016